T&S
10th International Conference on
TRANSPORT AND SEDIMENTATION OF SOLID PARTICLES
4-7 September 2000, Wroclaw, Poland, pp 497-510.

STEREOSCOPIC IMAGING MEASUREMENTS OF SOLID CONCENTRATIONS IN DENSE GRANULAR FLOWS

By B. Spinewine[1,2], H. Capart[1,3] and Y. Zech[1]

[1] *Department of Civil Engineering, Université catholique de Louvain, Place du Levant 1, B-1348 Louvain-la-Neuve, Belgium.*
[2] *Programme FIRST, Région Wallone, Belgium*
[3] *Fonds National de la Recherche Scientifique, Belgium*

The paper outlines imaging methods developed for the measurement of volumetric granular concentrations in the vicinity of a transparent interface. The aim is to construct an imaging indicator which remains robust and sensitive across the whole range of concentrations, and in particular in the dense limit. As monocular (i.e. single camera) techniques have been found in past attempts to present inherent limitations, the present work resorts to a stereoscopic principle. Efficient techniques based on the 2D Voronoï diagram and the epipolar line concept are first developed to reconstruct the three-dimensional positions of visible grains from pairs of digital images. Concentration is then estimated from these three-dimensional positions, using the 3D Voronoï diagram to homogenise the discrete data and obtain a near-wall estimate which is not biased by occlusion effects. The approach is validated using fluidisation cell tests. The comparison between bulk measurements and stereoscopic imaging estimators shows the latter to be endowed with both robustness and sensitivity across the whole examined range.

INTRODUCTION

Many flows of geophysical and industrial importance feature dense granular dispersions, the behaviour of which is known to be highly dependent on solid fraction. In dense conditions (around the random loose packing concentration $c_{s,\mathrm{rlp}} \approx 0.55$), small variations in solid fraction can change dramatically the rheological response of a particulate medium: the behaviour can vary from that of a solid-like elasto-plastic granular skeleton to that of a gas-like granular fluid (e.g. Savage, 1998; Aharonov and Sparks, 1999). The development of robust and sensitive methods for concentration measurements in such regimes is therefore highly worthwhile.

While particle imaging and particle tracking velocimetry have long been used in experimental fluid mechanics (for a review, see Adrian, 1991), it is only in recent years that imaging techniques have been adapted for granular flow applications (Capart and Young, 1998; Hsiau and Jang, 1998; Azanza et al., 1999; Capart et al., 2000; Lueptow et al., 2000). Two key advantages of imaging methods are their non-intrusive character and whole-field coverage. For dense, abrasive granular flows, intrusive probes will not only affect the flows but also be damaged by them, and a non-intrusive device is therefore an all-important requirement. Whole-field coverage, on the other hand, makes it possible to visualise flow structures with a degree of detail that is very difficult to match with point-wise probes or sensors. These advantages make imaging methods very attractive for velocimetry measurements, and provide a strong incentive for the development of corresponding techniques for the measurement of concentration.

T&S
10th International Conference on
TRANSPORT AND SEDIMENTATION OF SOLID PARTICLES
4-7 September 2000, Wroclaw, Poland, pp 497-510.

We consider the following situation of reference: a flowing three-dimensional dispersion of opaque, nearly identical grains is imaged through a viewing window or a free surface. Assuming that properties vary little in the direction normal to the transparent surface, the objective is to extract from digital images an estimate of the near-surface granular concentration. Indicators based solely on the geometry of the granular arrangements are sought, in order to avoid a strong dependence on illumination conditions (for luminance-based estimates, by contrast, see e.g. Kanda et al., 1999). This task becomes increasingly challenging as the concentration rises.

In such situations, monocular (single camera) imaging can be hoped to furnish some information about the volumetric concentration. For increasing concentrations, however, the effects of occlusion, excluded volume, and layering successively come into play and make the extraction of volumetric measurements from monocular images less and less feasible.

If the dispersion is highly dilute (and the unhindered depth of view is small, e.g. a thin slice of the flow is illuminated by a laser light sheet), then a trivial estimate of the volumetric number density can be obtained from monocular images by counting the number of viewed particle centres per unit image surface η and dividing by the depth Δz. This simple estimate breaks down quite rapidly as the concentration rises and occlusion effects intervene. As more and more grains are hidden from view by other grains, the surface density becomes less and less sensitive to the actual grain concentration c_s. For spherical particles assumed to be randomly distributed inside the viewing volume following a Poisson process, this effect can be quantified by the following relation (Capart et al., 2000):

$$\eta = \frac{4}{\pi D^2}\left[1 - \exp\left(-\tfrac{3}{2}\frac{c_s \Delta z}{D}\right)\right].$$

In this relation, D is the grain diameter and Δz is the considered depth of view, and it can be seen that the sensitivity of the surface density η to the volumetric concentration c_s decays rapidly with the ratio $c_s\Delta z\ /D$. In practice, therefore, the applicability of estimators based on surface density of particles on monocular images is restricted to volumetric concentrations below 10 %.

For higher concentrations, it is still possible to work with monocular images by considering pattern-based estimates. These are based on the observation that, for larger concentrations, excluded volume effects (i.e. the constraint that any one particle centre cannot penetrate a shell of one diameter around any other particle) induce certain preferential arrangements of the grains. On monocular images, this translates into two-dimensional patterns which are increasingly ordered as the concentration rises. Pattern-based estimators based on this idea have been introduced and tested in Capart et al. (2000), with reasonable results (but a limited sensitivity) for medium range concentrations up to the concentration of random loose packing $c_{s,\mathrm{rlp}} \approx 0.55$. The essential limitation of the approach is that it presupposes that local particle arrangements are statistically independent from the flow kinematics. This assumption, which corresponds to the postulate of "molecular chaos" adopted in kinetic theories of granular flow, is known to be reasonable in the collisional flow regime, when nearby-particle motions are decorrelated by random short-lived encounters with neighbouring grains. The assumption breaks down, however, in the denser frictional flow regime, when sustained contacts between particles induce the formation of a flow-dependent structure (e.g. layering).

A key point to be stressed is that the limitations of monocular methods are of a fundamental nature. If occlusion effects are significant and departures from molecular chaos are expected, no geometrically based monocular imaging method will work. These restrictions apply in particular to the dense frictional regime. To deal with the full range of concentrations, more information about the granular dispersion is needed than can be gathered from monocular images. Resorting to volumetric images (acquired with tomographic techniques such as magnetic resonance imaging, e.g. Nakagawa et al., 1993) provides one alternative. The sophistication, cost and limitations of the required apparatus, however, currently make this option impractical for most applications. Constituting a more accessible alternative, stereoscopic imaging is selected in the present work.

The stereoscopic method developed involves two main steps: stereoscopic matching, and concentration estimation. Starting with a pair of 2D images, the first step aims at pinpointing the three-dimensional positions of the visible grains. The second step consists in deriving from these discrete positions an estimator for the near-wall volumetric granular concentration. The remainder of the paper is structured as follows: a first section describes a tool which is used in both steps, namely the Voronoï diagram. The stereoscopic matching and concentration estimation techniques are then detailed. Finally, the methods are applied to fluidisation cell tests in order to validate the overall approach.

VORONOÏ DIAGRAM AND PROPERTIES

Consider a set of feature-points (e.g. particle centres) dispersed in a two-dimensional image plane or in a three-dimensional physical control volume. The Voronoï diagram is a geometrical construction which subdivides the space into a set of non-overlapping polytopes, or cells, surrounding each feature-point (see Figure 1). Each cell encompasses the region which lies closer to a given feature-point than to any other, e.g. with respect to Euclidean distance. The construction presents many useful properties which are discussed in a general context in Okabe et al. (1992). For imaging applications, three main properties are of particular interest.

Once constructed, which can be done very efficiently with methods such as Fortune's plane sweep algorithm (Fortune, 1987), the Voronoï construction can first be used to speed-up considerably multiple queries relative to neighbourhood relationships. The number of operations required for a nearest neighbour search, for example, becomes of the order of $n^{1/d}$, where n is the number of feature points and d = 2 or 3 is the number of dimensions, rather than of order n which would be obtained with a brute-force algorithm. In the present work, this property is used to speed-up the computationally intensive stereoscopic matching step.

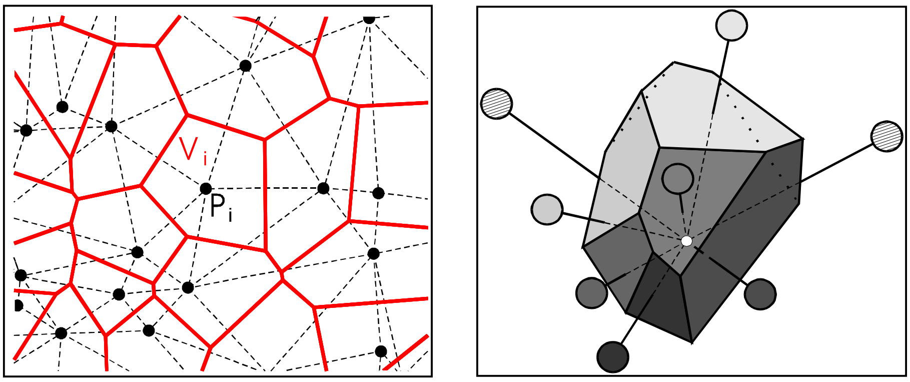

Figure 1: *Left*: Planar Voronoï diagram (——) and dual Delaunay tessellation (- - -). *Right:* A 3D Voronoï cell around feature point ○ ; to each natural neighbour ● corresponds a particular facet of the Voronoï polyhedron, perpendicular to the segment ●—○.

Secondly, the Voronoï construction can be used to homogenise quantities relative to individual feature-points, and thus to extend discretely sampled properties to full spatial coverage. The simplest such method is nearest-neighbour interpolation and consists in assigning to all points in a given cell the properties of its nodal feature-point. This property is used below to construct a robust estimate for the volumetric granular concentration.

Lastly, Voronoï cells can be used as patterns encapsulating information about the local arrangement of feature-points. This property can be exploited to construct robust pattern classification and pattern matching methods (Ahuja, 1982) and has been applied in particular by Capart et al. (2000) to the velocimetric matching of dense granular flows. It will not be used in the present work, but it is noted here to highlight the multipurpose usefulness of the Voronoï construction when both granular velocities and concentrations are sought.

T&S
10th International Conference on
TRANSPORT AND SEDIMENTATION OF SOLID PARTICLES
4-7 September 2000, Wroclaw, Poland, pp 497-510.

STEREOSCOPIC MATCHING

Stereoscopic imaging involves recording simultaneous images of a scene under two (or more) different viewpoints in order to obtain information about the depth (cross-image distance) of the visible features. With reference to Figure 2, consider two views of a flowing granular dispersion acquired using synchronised digital cameras (if particles are in motion, precise synchronisation of the two cameras is essential to avoid position-displacement ambiguities). The first step of the analysis consists in identifying grain centroids on each of the two images. Once characteristic points are located on each view, stereoscopic matching aims at recovering their positions in three-dimensional space.

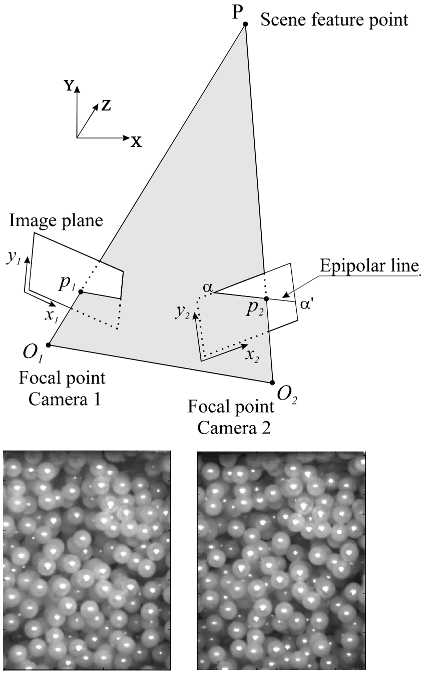

Figure 2 : *Top* : Stereo imaging principle. (X,Y,Z) = 3D world coordinates; (x_1,y_1) and (x_2,y_2) = 2D image coordinates. *Bottom* : two simultaneous views of the same scene.

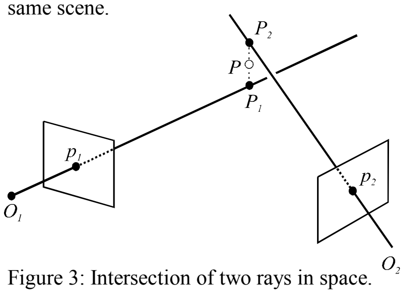

Figure 3: Intersection of two rays in space.

Stereoscopic matching can be conceptually broken down into two distinct tasks: the first involves the localisation of a feature-point (e.g. particle centre) in physical space (*X*,*Y*,*Z*) given its image co-ordinates under two calibrated viewpoints (x_1,y_1 and x_2,y_2); the second task is one of figuring out correspondence: for each feature point on the left-image plane, find the corresponding feature point on the right-image plane, so that both refer to one and the same physical particle. It turns out that projective geometry provides a single solution to both problems. The reason is that a pair of 2D views of a 3D dispersion of feature-points contains redundant information, which can be used to select the correct matches.

This geometrical problem can be handled neatly if one assumes that the projections are governed by affine geometry (e.g. Jain, 1995). An affine transformation covers projections from an arbitrary point onto a plane, and is characterised by preservation of straight lines. It accounts for several types of camera errors, but cannot model lens distortions. Affine properties are also preserved for refraction across flat interfaces between media of contrasting densities (e.g. air and water), as long as rays make sufficiently narrow angles with respect to the interface normal. If affine geometry is assumed, a relatively simple calibration step provides projection matrixes for each view, from which parametric ray equations can be associated to any point on either image. Physical feature-points P (Figure 3) then lie on the intersection of two rays originating from the focal point O_1 (resp.O_2) of each view and passing through paired image points p_1 (resp.p_2). In practice, imperfections in optics, calibration etc. prevent any two rays from perfectly intersecting each other even if they correspond to one and the same physical feature-point. The distance $\overline{P_1P_2}$ of closest encounter between any two rays, however, provides an indicator of the goodness-of-match between the corresponding pair of candidates on the two images.

An optimisation step can then be performed to select the global matching which minimises the sum of encounter distances over all candidate pairs, under the constraint that any one particle image on each view can be associated with no more than one particle image on the other view (this optimisation can be performed efficiently using the approximate Vogel algorithm, outlined e.g. in Capart et al., 2000). Once the global pairing is performed, the 3D position of each physical feature-point P can be estimated as the midpoint of the line segment P_1P_2 linking the points of closest encounter on the two corresponding rays.

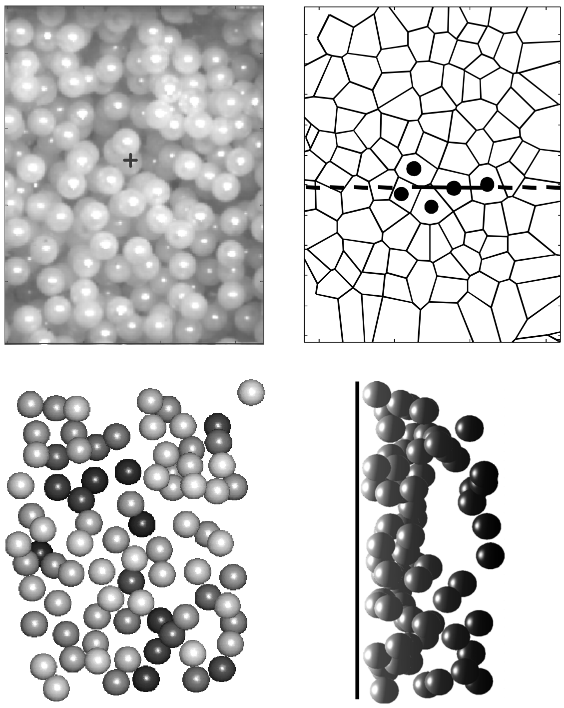

Figure 4 : Principle of epipolar stereoscopic matching. *Top left* : considered particle centre on image 1. *Top right* : corresponding epipolar line on image 2 (reduced to the segment in solid line), and identification of the match candidates. *Bottom* : reconstructed 3D positions of the particles. Colour is assigned according to depth (light for near-wall particles, darker for deeper ones). *Left* : front view. *Right* : side view.

A simple version of the above procedure (used for example in Douxchamps et al., in preparation) considers all possible pairs of image points as match candidates. When the number of particles rises, however, such a brute-force approach becomes prohibitively expensive in terms of computational time and memory allocation (the number of operations and memory spaces scales with n^2, where n is the number of particles). An alternative version was developed in the present work. It consists in exploiting epipolar lines and the Voronoï diagram to limit in advance the number of match candidates to be considered. The principle is illustrated in Figures 2 and 4, and can be described as follows.

If one assumes affine geometry, then each ray (e.g. O_1P) associated with a given image point (p_1) on one of the views is projected onto a straight line in the other view ($\alpha\alpha'$). This is the so-called epipolar line, which can be derived from the knowledge of the two projection matrixes and the image point position on the first view. Correct matches must fall in the neighbourhood of the epipolar line, and this can be exploited to preselect candidate pairs. One elegant way of performing this is to resort to the Voronoï diagram, and to retain as match candidates only the image points of the second view which have their 2D Voronoï cells pierced by the epipolar line (Figure 4b). Instead of considering as match candidates all the points in the image plane, one thus considers only a limited subset. Because of the way the Voronoï diagram is constructed, one is guaranteed that the nearest neighbour to the epipolar line (most likely to be the correct match) is retained among the subset. Furthermore, tracing of the epipolar line through the Voronoï diagram can be implemented in a very efficient way because the Voronoï construction encapsulates all the required neighbourhood relations. Finally, if a priori bounds are known for the depth range of the physical feature-points (e.g. the wall plane and a parallel plane at a maximum depth of view), then the epipolar line can further be restricted to an epipolar line segment, and the number of candidates diminished even more (solid line on Fig. 4d: only 5 match candidates). For the fluidisation experiments detailed below, implementation of this refined procedure yields a 20-fold speed-up of the computations over the brute-force algorithm.

CONCENTRATION ESTIMATION

Once particles have been positioned in space using the methods of the previous section, their volumetric concentration can be evaluated from the particle number density (i.e. the number of particle centres per unit volume). The most common way of obtaining such a number density from a discrete sample of points is by "binning". This method consists in subdividing the region of interest into separate compartments, or bins, counting the number of particle centres falling in each bin, and dividing this number by the corresponding volume. The main problem of the method lies in the choice of a suitable bin subdivision. If the granular dispersion is homogeneous (as in the fluidisation experiments reported hereafter), the only direction along which the apparent measured concentration might vary significantly -due to occlusion- is the one normal to the wall. Hence bins can be replaced by slices taken parallel to the transparent surface.

To illustrate the difficulty of choosing a suitable bin size in the present context, let us examine what occurs in the cases of thin and thick slices, respectively.

Results obtained when bins are taken as thin slices oriented parallel to the transparent wall are plotted in Figure 5a. The curves show the particle number distributions obtained as a function of depth (normal to the transparent surface), for two different particle concentrations inside the physical volume. Because of occlusion (particles in the front hiding from view particles in the back), the number density of visible particles diminishes with depth, and this decrease is steeper for higher concentrations. As a result, only the near-wall values (close to zero depth) faithfully reflect the volumetric concentration that would be obtained without occlusion. A second feature of the curves is noteworthy: their non-monotonous shape. Localised peaks, sharper for higher concentration, are obtained at intervals of the order of one grain diameter. This reflects an ordering effect induced by the walls, imposing a semi-crystalline arrangement of the grain centres when the packing is dense. (For high concentrations, this inter-distance should approach the theoretical value of $\sqrt{2}/2.D$, corresponding to the 'cannonball' hexahedral arrangement of particles. This is in nearly perfect accordance with the measured distance between successive peaks for the highest obtained concentration of 57 %). While this feature is interesting in itself (and shows the resolving power of the stereoscopic matching technique), it constitutes a second-order effect when one is interested in the mean volumetric concentration rather than in the details of the near-wall microstructure. Thin slices, therefore, provide too much detail.

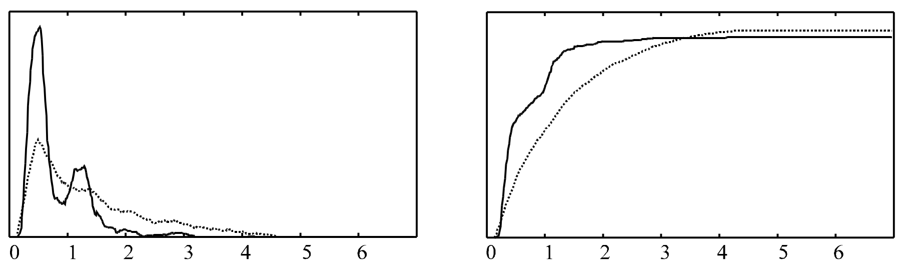

Figure 5 : Experimental distribution of visible particles centres in function of the depth (normal to wall) for two characteristic concentrations (solid line corresponds to an average solid fraction of 57 %, dotted line to 26 %). Wall position corresponds to the left of the graphs, intervals between successive graduations on the horizontal axis correspond to one particle diameter. *Left* : local particle density. *Right* : cumulative number of visible particles.

Figure 5b presents the corresponding cumulative distribution curves. The asymptotes of these curves correspond to the results that would be obtained for one single bin corresponding to a very thick slice parallel to the wall. By integrating over depth, we are in fact counting the number of particles visible on two-dimensional images. What is shown is that the resulting surface density constitutes a very poor indicator of the actual volumetric concentration inside the physical volume. Because of occlusion effects, almost indistinguishable asymptotes are obtained for two very different concentrations.

This is precisely the result sketched in the introduction: because of occlusion, the surface density of visible particles on 2D images becomes insensitive to the actual volumetric concentration. Thick slices, consequently, cause a loss of resolution.

To avoid such problems, and to generalize to non-uniform concentrations along directions parallel to the interface (for which slices are inadequate), it is natural to seek mid-sized bins, with a size and shape adapted to the granular character of the dispersion. Voronoï cells constitute natural candidates for such medium-sized bins. The proposed concentration indicator, based on the three-dimensional Voronoï diagram, is based on the following three steps.

At each node of the Voronoï diagram (i.e. at each particle position), concentrations are first defined in a natural way by dividing the particle volume by the volume of the surrounding Voronoï cell. When constructing the Voronoï diagram, particular attention is given to the specification of boundary conditions: in order to account implicitly for the presence of the transparent wall, Voronoï cells are truncated at the interface by adding mirror virtual points on the outer side. Far away from the wall, on the other hand, unbounded cells having vertices at infinity have their concentration naturally set to zero. This step provides a set of volumetric concentration values dispersed in the 3D volume at the discrete particle positions.

Secondly, the concentration data relative to individual particles are extended over a regular grid, using nearest-neighbour interpolation. The local concentration at a given feature point is assigned to all the points inside its Voronoï cell. Again, the Voronoï diagram is used to speed up nearest-neighbour search queries. This gridding procedure is important to perform consistent spatial averages, and to be able to compare image acquired at different time steps, for which the overall concentration is unchanged but the internal arrangement of particle positions has been altered.

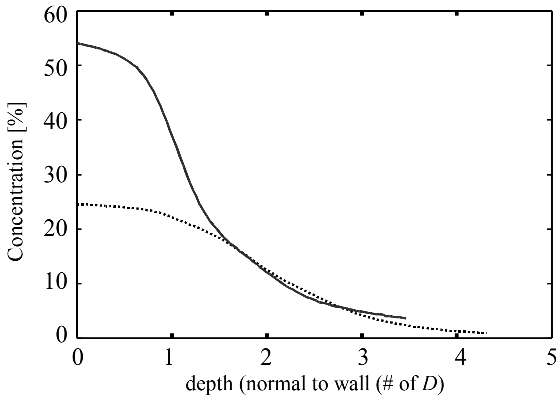

Figure 6 : Experimental profile of the Voronoï-based concentration estimator across the depth (normal to the wall), for the same two bulk concentrations (solid line : 57 %, dotted line : 26 %). Wall position on the left, intervals between graduations on the horizontal axis correspond to one particle diameter.

Thirdly, spatial averages are performed along chosen axes to homogenise volumetric concentration measurements, which have an intrinsic discrete character. Special care has to be taken to account for occlusion effects, which will cause the measured concentration to reduce progressively along the depth due to a decreasing number of visible particles. As occlusion acts in the direction normal to the transparent surface, consistent averages can be performed along planes parallel to the wall. Typical curves for the resulting apparent concentration profile as a function of the depth are plotted on figure 6 : they are characterised by a horizontal tangent near the wall and an asymptotic decrease towards zero for larger depths. Such profiles are more stable than those of figure 5a, and can be used to provide a robust estimate for the near-wall concentration. Although it is possible that information from the full depth-varying curve can be of use, in the present work the concentration indicator chosen is the wall intercept of the concentration curve.

FLUIDISATION CELL TESTS

Fluidisation cell experiments were undertaken to test the proposed methods and validate the resulting concentration measurements. The experimental set-up is presented on figure 7, and consists in a cylindrically shaped cell fitted with a plane rectangular window (in order to obtain non-distorted images). Inside the cell, a static arrangement of identical spheres is subjected to an upward fluid flux. Net gravitational force on the granular phase is counterbalanced by upwards acting drag forces, causing the granular mixture to expand vertically. If special care is taken to insure uniformity of the fluid velocity distribution and vertical orientation of the set-up, a homogenous dispersion of randomly moving grains is observed in the cell. A wide range of well-controlled concentrations can obtained by simply adjusting the fluid discharge.

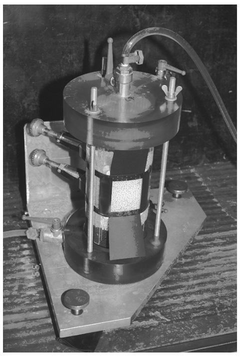

Fluidisation cell :
Inner diameter : 10 cm; Height : 25 cm
Rectangular plane window : 5 × 10 cm.

Particles used :
identical reflecting spheres,
diameter : 6.1 mm
relative density : 1.048

Imaging set-up :
2 synchronised digital cameras
resolution : 256*256 pixels
256 grey levels.

Test #	1	2	3	4	5	6	7	8	9	10	11
Fluidisation velocity [cm/s]	1,91	1,02	2,39	1,73	2,14	2,47	0,90	0,70	1,15	1,79	2,86
Bulk concentration [%]	36,8	50,6	29,9	39,4	32,7	28,4	54,1	57,3	42,2	37,2	25,8

Figure 7 : Experimental set-up and conditions of the 11 performed tests.

T&S
10th International Conference on
TRANSPORT AND SEDIMENTATION OF SOLID PARTICLES
4-7 September 2000, Wroclaw, Poland, pp 497-510.

A series of 11 tests has been carried out, for the experimental conditions summarised in figure 7. The concentration ranged from 26% for the highest fluidisation velocity to 57% for the lowest one. Bulk measurements of the volumetric concentration were derived from the height of the fluidised bed (with a known volume of material placed inside).

For each test, 16 pairs of images from two synchronised cameras were acquired, separated by time intervals sufficiently large to avoid spatial correlations of the particle positions between successive images. Imaging estimates for the volumetric concentration were derived from each pair of images according to the methods outlined above. The obtained near-wall concentration was finally averaged over the 16 images available for each test. Results are presented on figure 8.

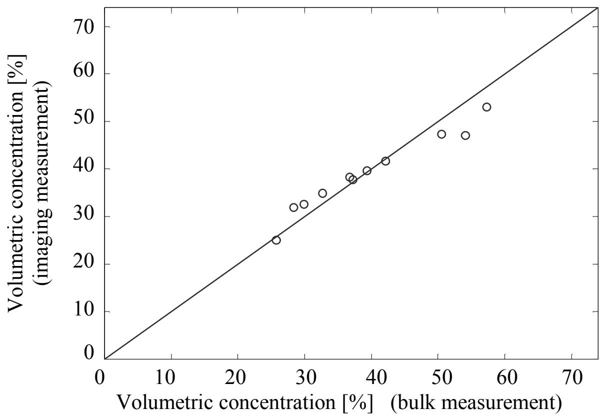

Figure 8 : Comparison of the concentration values obtained by bulk measurements and by stereoscopic digital imaging. The theoretical solid line corresponds to perfect agreement.

Good quantitative agreement is obtained. A remarkable property of these results is the absence of any calibration coefficient, offering a potential direct method for measurement of solid concentrations by means of non-intrusive digital imaging.

CONCLUSIONS

In the present work, a novel non-intrusive method was developed for the experimental measurement of near-wall solid concentration in granular flows. The method includes an efficient stereoscopic imaging algorithm, used to pinpoint the 3D positions of visible particles. The 3D Voronoï diagram is then exploited to derive a concentration estimator which remains robust and sensitive across the whole range of concentrations. In particular, the method applies to the dense limit, where occlusion, excluded volumes and layering effects make it very difficult to obtain volumetric measurements from monocular images. As it relies only on direct observations of particle positions, the method requires no calibration procedure. Successfully validated in fluidisation cell experiments performed with idealised particles, the methods remain to be tested on more complex granular flows, as well as flows involving more complex grains.

REFERENCES

Adrian, R. J. (1991). Particle-imaging methods for experimental fluid mechanics. *Annual Review of Fluid Mechanics* 23: 261-304.

Aharonov, E., Sparks, D. (1999). Rigidity phase transitions in granular packings. *Physical Review E* 60: 6890-6896.

Ahuja, N. (1982). Dot pattern processing using Voronoï neighbourhoods. *IEEE Transactions on Pattern Analysis and Machine Intelligence.* 4: 336-343.

Azanza, E., Chevoir, F., Moucheront, P. (1999). Experimental study of collisional granular flows down an inclined plane. *Journal of Fluid Mechanics* 400: 199-227.

Capart, H., Young, D.L. (1998). Formation of a jump by the dam-break wave over a granular bed. *Journal of Fluid Mechanics* 372: 165-187.

Capart, H., Young, D.L., Zech, Y. (2000). Voronoï imaging methods for the measurement of granular flows. Submitted to *Experiments in Fluids*.

Douxchamps, D., Devriendt, D., Capart, H., Craeye, C., Macq, B., Zech, Y. Three-dimensional reconstruction of the oscillatory free-surface of a flow over antidunes: stereoscopic and volumetric techniques. In preparation.

Fortune, S. (1987) Fluid particle model. *Phyical Review E* 57: 2930-2948.

Hsiau, S. S., Jang, H. W. (1998). Measurements of velocity fluctuations of granular materials in a shear cell. *Experiments in Thermal and Fluid Science* 17: 202-209.

Jain, R., Kasturi, R., Schunck, B.G. (1995). *Machine Vision*. McGraw-Hill, Inc., New York, N.Y.

Kanda, T., Miyamoto, H., Iwami, S. (1999). Measurement of suspended solid concentration by using image processing technique. *XXVII IAHR Biennal Congr.*, Graz, Aug. 1999, Abstract p. 253, full paper on CD-Rom proceedings.

Louge, M. Y., Jenkins, J.T. (1997). Microgravity segregation in binary mixtures of inelastic spheres driven by velocity fluctuation gradients. In *Mechanics of deformation and flow of particulate materials* (eds Chang, C.S., Misra, A., Liang, R.Y., and Babic, M.), ASCE, pp. 370-379

Lueptow, R.M., Akonur, A., Shinbrot, T. (2000). PIV for granular flows. *Experiments in Fluids* 28(2): 183-186.

Nakagawa, M., Altobelli, S.A., Caprihan, A., Fukushima, E., Jeong, E.K. (1993) Noninvasive measurements of granular flows by magnetic-resonance-imaging. *Experiments in Fluids* 16: 54-60

Okabe, A., Boots, B., Sugihara, K. (1992). *Spatial tessellations: concepts and applications of Voronoi diagrams*. John Wiley & Sons, Ltd., Chichester, U.K.

Savage, S.B. (1998). Analyses of slow high-concentration flow of a granular material. *Journal of Fluid Mechanics* 377: 1-26.